Hindawi Publishing Corporation
Journal of Combustion
Volume 2015, Article ID 817259, 11 pages
http://dx.doi.org/10.1155/2015/817259

Research Article

Experimental Study of Constant Volume Sulfur Dust Explosions

Joseph Kalman,[1,2] Nick G. Glumac,[1] and Herman Krier[1]

[1] *University of Illinois at Urbana-Champaign, 1206 W. Green Street, Urbana, IL 61801, USA*
[2] *Naval Air Warfare Center Weapons Division, 1 Administration Circle, China Lake, CA 93555, USA*

Correspondence should be addressed to Joseph Kalman; kalmanjm@gmail.com

Received 8 November 2014; Accepted 29 January 2015

Academic Editor: Hong G. Im

Dust flames have been studied for decades because of their importance in industrial safety and accident prevention. Recently, dust flames have become a promising candidate to counter biological warfare. Sulfur in particular is one of the elements that is of interest, but sulfur dust flames are not well understood. Flame temperature and flame speed were measured for sulfur flames with particle concentrations of 280 and 560 g/m^3 and oxygen concentration between 10% and 42% by volume. The flame temperature increased with oxygen concentration from approximately 900 K for the 10% oxygen cases to temperatures exceeding 2000 K under oxygen enriched conditions. The temperature was also observed to increase slightly with particle concentration. The flame speed was observed to increase from approximately 10 cm/s with 10% oxygen to 57 and 81 cm/s with 42% oxygen for the 280 and 560 g/m^3 cases, respectively. A scaling analysis determined that flames burning in 21% and 42% oxygen are diffusion limited. Finally, it was determined that pressure-time data may likely be used to measure flame speed in constant volume dust explosions.

1. Introduction

Sulfur dust cloud combustion is a potential candidate to counter biological weapons. Sulfur dust has been used as a pesticide [1]. However, the more intriguing aspect of sulfur dust clouds is that they produce sulfur oxides which are chemical precursors to sulfuric acid [1]. It is well-known that sulfuric acid is extremely corrosive and dangerous to living organisms. The concept is that burning sulfur clouds will produce sulfur oxides. In the presence of water, sulfuric acid can be formed. It is thought that the sulfuric acid created, coupled with the elevated temperatures and ultraviolet radiation produced, will kill the spores. Other strong acids have been shown to have sporicidal tendencies [2].

In recent years, compositions have been studied for biodefeat applications. Mechanical alloys of aluminum and iodine [3, 4] as well as aluminum-iodine pentoxide thermites have been studied [5] and shown to be effective in killing biological spores, at least in part, due to the release of iodine. Other mechanical alloys of titanium and boron have also been investigated for this purpose [3, 6, 7].

Fundamentally, sulfur dust flames are unique. Sulfur is one of two elemental dusts whose combustion products are gaseous at standard conditions (298 K, 1 atm) with carbon being the other. Unlike carbon, the melting and boiling points of sulfur are much lower than the adiabatic flame temperature of a sulfur-air flame. This combination of factors provides conditions for a dust flame with a potentially strong gas-phase component.

To date, very few studies have investigated sulfur dust clouds. The limited work on sulfur dust flames by Proust [8] is among the only publications to do so; however, that work has provided few details into the combustion mechanism. Therefore, the primary goal for the current work is to measure fundamental aspects of sulfur dust cloud combustion in terms of fundamental quantities (e.g., flame speed) and to gain insight into the physical and chemical mechanisms involved. Moreover, the use of pressure-time data from constant volume dust explosions to determine flame speed is investigated.

2. Experimental Methods

The current study uses a 31 L cube chamber to maximize optical access. Five of the sides (including the door) have acrylic windows with circular viewing areas of 6.7 in diameter. Each

window is clamped onto the side of the chamber with a size 6 pipe flange. Gas, vacuum, and pressure transducer ports are located on the top and sides of the chamber. A piezoresistive Kulite pressure transducer (XTM-190-250G) is used, and the signals are conditioned by an Endevco PR Conditioner model 106. The bottom (sixth side) has five 1 in diameter ports. One port is placed in the center with the other four being 3 inches away from the center, each in a different direction (i.e., left, right, front, and back). A single off-center port is used for wire feedthrough for the ignition source.

The port in the center of the chamber has a nozzle with forty, 0.889 mm diameter holes (number 65 drill bit) at a 45 degree angle. The two-piece particle injector is mounted underneath the center port of the chamber. The first piece is attached to the chamber through 1/4 in-20 screws. It contains a port on the side that attaches to a compressed air line and 1/4 in stainless steel tube which extends to the center and is bent 90 degrees downward. The powder is placed in an aluminum holder with a conical bottom (from a 1 inch drill bit) that attaches to the second piece of the injector. The centered 1/4 inch tube elbow directs the air burst downward into the powder holder. The pressurized burst rebounds off the bottom of the powder holder and carries the particles upwards through the nozzle into the chamber. The chamber is sealed by o-rings on the windows, injector, and door. Additional descriptions of the chamber are provided in [9].

Sulfur powder (−325 mesh) from Alfa Aesar was used. Particle size analysis was conducted using a Jeol 6060LV scanning electron microscope (SEM). The particles had an average diameter of 22.4 μm with a Sauter mean diameter of 30.4 μm. An anticaking agent, Aerosil 200 (Evonik), was used to improve the dispersion characteristics of sulfur. The average diameter of the Aerosil 200 powder was 12 nm according to the manufacturer. A size distribution was not measured as the particles were too small to be resolved by the SEM. The sulfur was mixed with 1% of Aerosil 200 by mass in a low energy tumbler for 3 hours. The addition of the anticaking agent was observed to have a noticeable effect on the flowability and dispersal of sulfur. Further details on the choice of anticaking agent are given in [9].

A known mass of the sulfur mixture was placed within the injector. The mass of powder remaining in the injector after the test was measured to determine the actual amount of powder injected. Alligator clips on the ignition posts held the igniter in the center of the chamber. A 4 J igniter (pyrogen covered bridgewire, Estes) was used to initiate combustion. The charge was ignited by discharging a 1 μF capacitor at 4000 V from an RISI fireset (Model FS-43).

Prior to the test, the chamber was put under vacuum and filled to slightly below atmospheric pressure (2 in Hg) so that the gas used for injection brought the total pressure to 1 atmosphere. A 100 psig burst of air was used to inject the powder. The injection lasted a total of one second under constant pressure. Ignition occurred 400 ms after injection had ended to allow for a uniform cloud to form and turbulence to dissipate.

The determination of this ignition time was made by analysis of two-dimensional particle concentration measurements. These laser extinction measurements provided quantitative information on how the particle concentration developed in time and space. The pixel intensities from images taken prior to powder injection were averaged and used as the incident intensity, I_0, in Beers Law:

$$\frac{I}{I_0} = \exp \frac{-3Q_{\text{ext}}LC}{2\rho D_{32}}. \quad (1)$$

The intensity of each pixel in subsequent images allowed for the particle concentration, C, to be determined since the extinction efficiency (Q_{ext}) from Mie theory, Sauter mean diameter, D_{32}, path length, L (355 mm), and density of sulfur, ρ were all known. The arithmetic mean and standard deviation of the particle concentration for all pixels were calculated to provide a statistical analysis of the uniformity of the cloud. The ignition time was taken as the point in time where the spatially averaged concentration approached the expected value (based upon the amount of powder injected) and the standard deviation approached a minimum or decreased.

This method also provided visual evidence of the turbulence dissipating. Although the turbulence was never directly measured, it is believed that this quantitative measurement of the particle concentration yields sufficient insight into the injection process. Moreover, all of the experimental conditions in this work have the same injection and ignition conditions (e.g., ignition delay and injection back pressure). Comparison of the results from each conditions should see minimal effects from the turbulence. The reader is directed to [9] for additional details and discussion on these measurements.

2.1. Diagnostics. Flame speed measurements were made with ionization probes, similar to the work of Nair and Gupta [10], but were applied to dust flames instead of the gaseous flames that they studied. Two of the off-center 1 in diameter holes were used to feedthrough wires for the ionization probes where the wires were terminated by an R-type thermocouple connector (Omega). Two 0.01 in diameter tungsten wires were fed through a two-bore, 1/8 in outer diameter aluminum oxide tube. Approximately 1/4 inch of each wire extended outside of the ceramic tube. The other end of each wire was attached to the complementary thermocouple connector. The placement of the ionization probes are shown in Figure 1 where the relative location of the two ionization probe combs were chosen to provide information of the symmetry of the flame. The distance between the probes in each comb was 15.5 ± 0.76 mm.

Signals were recorded using a pair of Picoscope 4424 oscilloscopes, which collected 200,000 samples over a 2-second period. A pair of ionization probe traces from a sulfur flame is shown in Figure 3. The time when the first voltage drop reached a minimum for each trace was taken as the time when the flame front reached the probe. Laser shadowgraph confirmed this arrival qualitatively, as shown in Figure 2. The red curve indicates the location of the flame front. This feature was observed to reach the ionization probe at the same time (i.e., within the temporal resolution of the camera) the voltage trace spiked from the ionization probe (Figure 3).

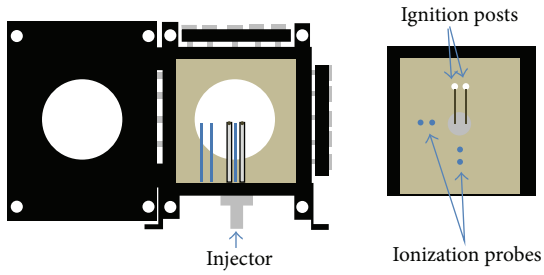

Figure 1: Schematic of the flame speed experimental setup.

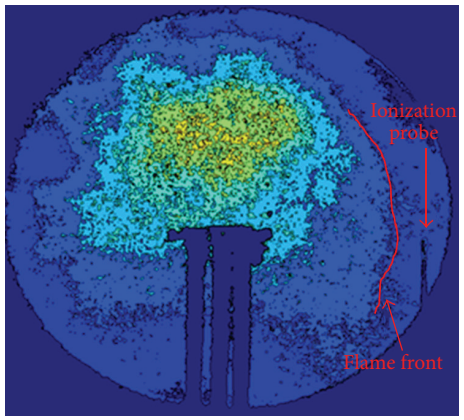

Figure 2: Qualitative shadowgraph measurement used to verify the time-of-arrival of the flame to the ionization probe. Image was taken prior to the flame reaching the probe.

The shadowgraph measurement also provided qualitative information on the flame shape. Although portions of the front are smooth, the flame front is not symmetric. The cause of this appearance is likely a combination of remaining turbulence and natural convection.

The Δt shown in Figure 3 was used to calculate the flame speed. An uncertainty of 20% of the nominal value was associated with each measurement which is mostly due to the time-of-arrival measurement. The density corrections were calculated using Cantera [11] and the SOx mechanism from the University of Leeds [12].

Temperature measurements were made using thermocouples and pyrometry. Thermocouples (50 μm R-type, Omega part P13R-002) were covered in a thin coating of an aluminum oxide spray paint (ZYP Coating, A aerosol) to minimize catalytic effects. Thermocouples were attached to the connectors within the dust explosion chamber in the same manner as the previously described ionization probes. The thermocouple extension wire was connected to an Omega data acquisition (DAQ) system (Omega part OMB-DAQ-3005). Temperature was sampled every 100 μs for the first 2 seconds of each test. The DAQ system was triggered by a TTL pulse generated by the delay generator. The measurements were corrected for radiative and conductive losses.

Pyrometry measures the temperature of the condensed phases by comparing the thermal background to Planck's equation (with the emissivity included). A three-color

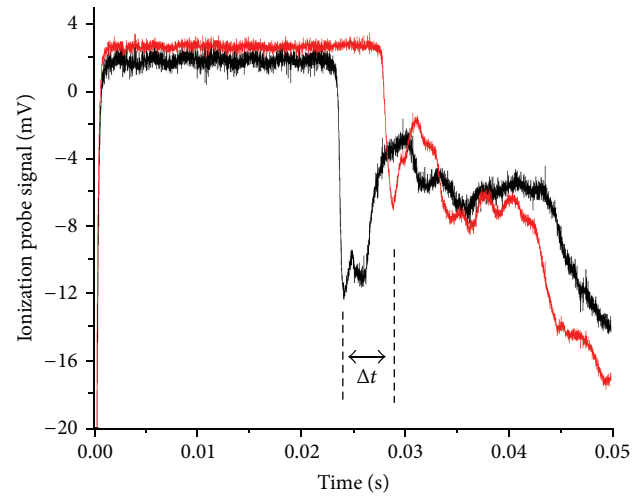

Figure 3: Representative voltage traces from the ionization probes from a sulfur flame.

pyrometer was used to obtain time-resolved temperature information by monitoring the emission at 700, 825, and 900 nm. Hamamatsu R928 photomultiplier tubes (PMT) were used for the 700 and 825 nm channels, while an R636-10 PMT was used for the 900 nm channel. Light was collected into a trifurcated fiber optic cable where each of the three branches went to a different PMT. A Stanford Research System (SRS) 300 MHz quad preamplifier (SRS model SR445) conditioned each signal before being recorded by the Picoscope.

A fiber optic-coupled Ocean Optics Jaz spectrometer was also used for pyrometry measurements. This spectrometer records spectra from 200 to 870 nm. However, due to spectral features from SO, SO_2, and S_2 from the ultraviolet into the visible region of the spectrum, only the thermal emission in the range of 600 to 850 nm was used to determine the condensed phase temperature. The intensity calibration for both devices was conducted with a tungsten lamp (Ocean Optics LS Cal 1) with a known spectral intensity for the spectral regions studied.

3. Results and Discussion

Measurements of pressure rise, temperature, and flame speed were made for 6 different conditions. Two different concentrations of the sulfur/anticaking agent mixture were used (280 and 560 g/m^3) and three different concentrations of oxygen (10, 21, and 42% by volume). The remaining balance of the gas was nitrogen. The stoichiometric conditions were 280 g/m^3 in 21% oxygen and 560 g/m^3 in 42% oxygen. The choice of these conditions was based upon consideration of the application (i.e., burning in air) and being able to isolate the effects of particle concentration and stoichiometry. Difficulties establishing flames at lower particle concentrations prevented the use of those concentrations. The tendency of sulfur to agglomerate, especially at the higher sulfur concentrations, yielded an upper limit on the particle concentrations used.

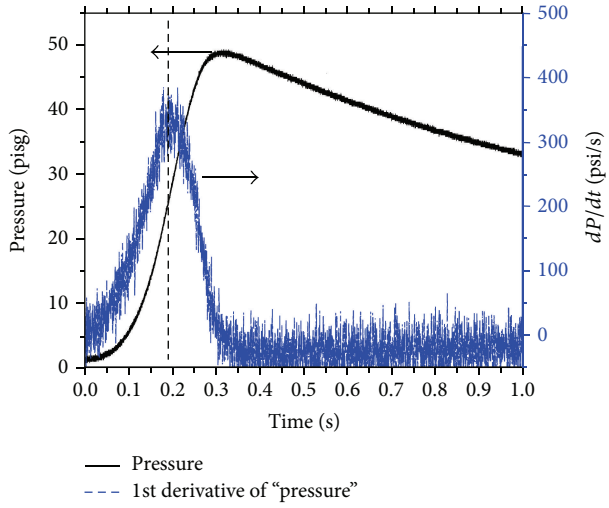

FIGURE 4: Sample pressure-time data from a sulfur explosion.

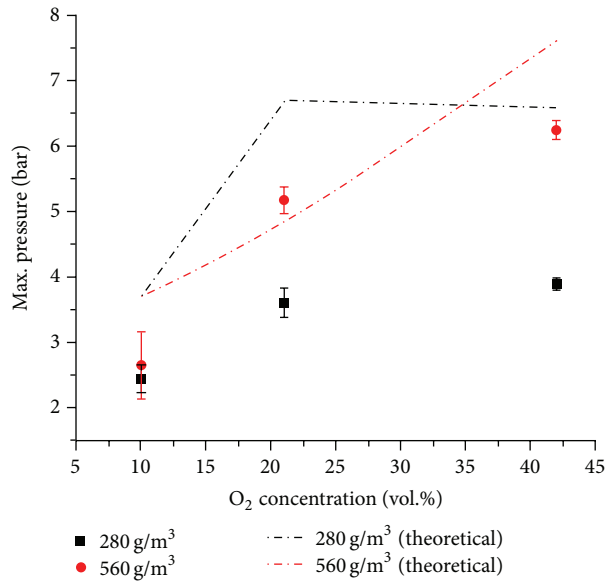

FIGURE 5: Maximum pressure rise (absolute pressure) for sulfur explosions within a 31 L chamber.

The problem of agglomeration is addressed in greater detail in [9].

3.1. Pressure Data. A representative pressure-time curve and its first temporal derivative are shown in Figure 4. The maximum pressure rises are shown in Figure 5 with the theoretical maximum pressure rise and were determined from NASA's CEA program [13] under constant volume. It was observed that the pressure rise increased with particle concentration and increasing oxygen concentration. The data is consistent with work by Cashdollar [14] after scaling their pressure data to account for the different chamber volumes between the facilities used in each respective study.

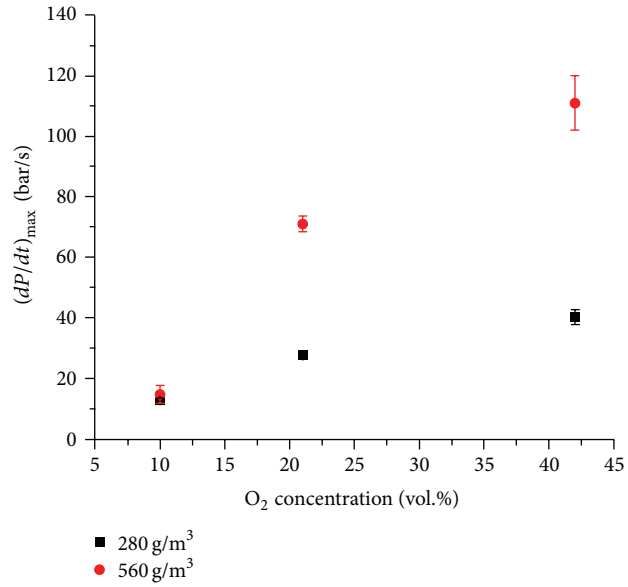

FIGURE 6: Maximum rate of pressure rise (absolute pressure) within the 31 L chamber from sulfur explosions.

The 560 g/m^3 condition within a 21% oxygen environment resulted in a pressure rise greater than the maximum pressure. This result may be due to particle settling from increased agglomerations during the experiment. An increase in agglomerations at the higher particle loadings were reported in [9]. If additional particles fall out of the suspension, it will bring the equivalence ratio closer to stoichiometric for these conditions. The maximum pressure will increase and approach the value seen for the lower particle loading. A similar effect of particle settling should then be expected for the 10% and 42% oxygen conditions. The difference in the maximum pressure rise for 10% O_2 is negligible because the maximum theoretical pressure rises are almost identical. Figure 5 shows that the maximum pressure (dashed lines) in the oxygen enriched case would be lower if the particle settling increased. This decrease is consistent with what was observed experimentally. For all of these conditions, it is challenging to quantify how much the pressure should change theoretically because the actual mass of settled particles is unknown.

The maximum rate of pressure rise, Figure 6, was seen to increase monotonically with oxygen concentration. For oxygen concentrations above 10% by volume, the rate of pressure rise is greater for higher particle concentration. The rate of pressure rise indicates how quickly the heat is being release. The importance of this quantity will be seen in (2), where the rate of maximum pressure rise is directly proportional to the flame speed.

3.2. Validity of Pressure-Time Data for Flame Speed Measurements. Pressure-time data may also be used to determine flame speed. Dahoe and de Goey [15] analyzed constant volume explosions (not necessarily dust explosions) from

a thermodynamic standpoint to relate pressure-time data to laminar flame speed. This equation is shown as

$$\frac{dP}{dt} = \frac{3}{R}\left(\frac{dx}{dP}\right)^{-1}\left[1-\left(\frac{P_i}{P}\right)^{1/\gamma}(1-x)\right]^{2/3}\left(\frac{P}{P_i}\right)^{1/\gamma} S_L, \quad (2)$$

where

$$x(P) = \frac{P - P_i}{P_e - P_i} \quad (3)$$

and P is the instantaneous pressure, P_i and P_e are the initial and maximum pressures, respectively, and R is the spherical equivalent radius taken to be the radius of sphere with the same volume as the chamber used in the current study. The ratio of the specific heats, γ, was assumed to be constant (and approximately equal to 1.4 here because of the use of air), and S_L is the laminar flame speed. The analysis Dahoe and de Goey [15] conducted on this method included the additional assumption of a linear dependence on pressure for the mass burnt fraction, $x(P)$ (3). The work by Luijten et al. [16] used a multizone approach to develop a more rigorous definition for x, although it is not shown here because of its length.

The derivation of (2) was based on ideal assumptions that in practice may not be true for dust explosions. They are as follows.

(1) The chamber is well-insulated and assumed to be filled with reactants that are perfectly mixed and stagnant.

(2) The mixture is ignited from the center and the flame front produced is spherical, infinitely thin, and not wrinkled.

(3) The flame front breaks the chamber into two regions, the burnt and unburnt gases, where the mixtures within each zone are uniform (e.g., composition and temperature).

(4) Since the chamber has a fixed volume and heat cannot escape due to the well-insulated walls, the pressure rises from the heat addition. Moreover, the hot combustion products within the spherical flame will expand, thus compressing the unburnt gas isentropically.

Two concentrations of the sulfur mixture were tested to determine if the use of pressure-time data to measure flame speed is appropriate for dust explosions. A near stoichiometric concentration of 264 ± 34 g/m^3 and a fuel-rich condition of 498 ± 53 g/m^3 were ignited in air by a pyrotechnic igniter. Energy release by the igniter did not have a significant influence on the measurement [9]. The uncertainty in the concentration is due to the distribution of the measured powder mass injected.

The two combs of ionization probes discussed above were used to directly measure the flame propagation speed and compared to those calculated from (2) and (3). The calculated flame speed based upon the pressure-time data shown in Figure 4 is displayed in Figure 7.

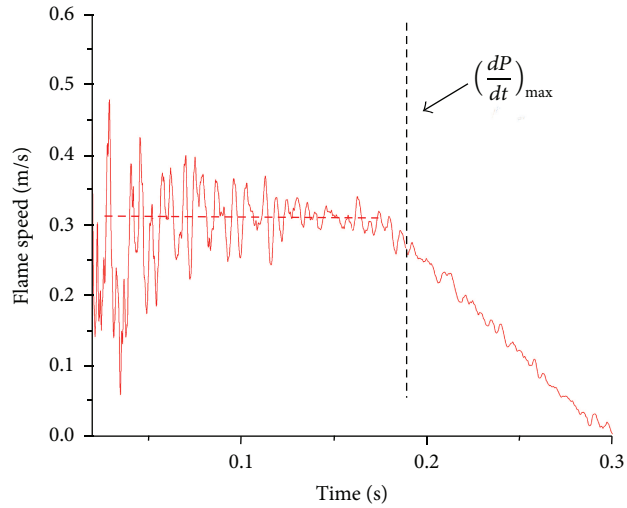

Figure 7: Calculate flame speed from pressure-time data.

The calculated laminar flame speed initially oscillates significantly due to a low signal-to-noise ratio from the pressure transducer signal. These oscillations dampen as the pressure rises. Despite the oscillatory nature, each calculated curve was observed to oscillate around a constant value until the time where dP/dt is a maximum. The time of the maximum rate of pressure rise is indicated by the vertical lines in Figures 4 and 7. The laminar flame speed from the pressure data was taken as the average speed from 20 ms after ignition to the time where $(dP/dt)_{\max}$ was reached. The time of 20 ms was used to limit the influence of the low signal-to-noise ratio of the pressure data very close to the instant of ignition. The decrease in laminar flame speed after $(dP/dt)_{\max}$ was also observed by Santhanam et al. [17]. The reason for the decrease in flame speed is very likely due to heat losses. As the flame approaches the walls of the vessel, additional heat is lost to those walls which are near room temperature. The rate of pressure rise, which is related to the rate of heat release, decreases because some of that energy is absorbed by the chamber walls. The rate of pressure rise is proportional to flame speed (see (2)) so that a decrease in flame speed is observed. An analysis on the primary mode of heat transfer from the flame is discussed in the following section.

3.2.1. Heat Loss Analysis. The decrease in flame speed after $(dP/dt)_{\max}$ was believed to be due to heat losses. With the increased amount of thermal radiation from dust flames, it is necessary to determine the importance of the various modes of heat transfer, specifically conduction and radiation.

The amount of energy lost to the chamber walls is difficult to quantify because of the complexity of the problem. However, the relative importance of conduction versus radiative losses may be analyzed qualitatively. The ratio of conductive to radiative losses, (4), was approximated for different flame temperatures and location (i.e., distance between the flame and the wall) where k is the thermal conductivity, ϵ is the emissivity, σ is the Stefan-Boltzmann constant, Δx is

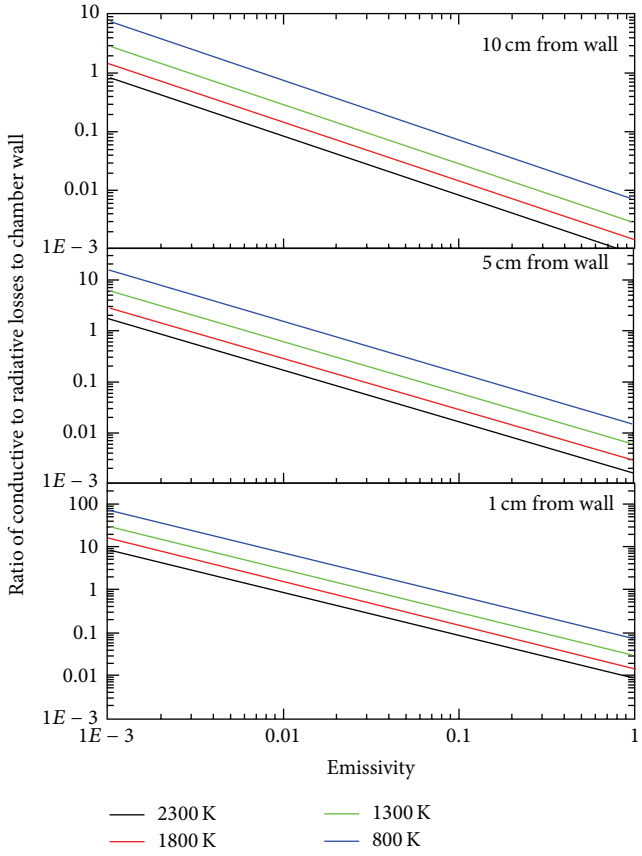

Figure 8: Calculated (first-order approximation) ratio of the conductive and radiative heat losses at multiple positions, at flame temperatures, and for $F = 1$.

the distance between the flame and the wall, and T is the temperature at the location indicated by its subscript. The variable F is the ratio of the surface area of the particles within the flame and flame front surface area. Since the emissivity of the powder is unknown, the ratio of the heat losses was calculated as a function of emissivity. Figure 8 shows the results from these calculations. Consider

$$\frac{Q_{\text{cond}}}{Q_{\text{rad}}} \approx \frac{k}{F\epsilon\sigma} \frac{(T_{\text{flame}} - T_{\text{wall}})}{\Delta L} \frac{1}{T_{\text{flame}}^4 - T_{\text{wall}}^4}. \quad (4)$$

The calculated ratios displayed in Figure 8 assumed the ratio of the particle surface area to that of the flame was unity. This assumption is not realistic since the particles only constitute a fraction of the flame front for a given flame thickness. The value of F can be determined using geometric considerations, an average particle diameter, and a flame thickness. Santhanam et al. [17] calculated the flame thickness of Al dust flames by multiplying the flame speed by the burntime of an individual Al particle. This same estimation is more challenging for sulfur dust since the burn time of an individual particle is unknown. The effect of flame thickness will be discussed.

High temperatures and large values of the emissivity favor radiative dominated heat losses when $F = 1$, which is to be expected since thermal radiation is dependent on those two parameters. For most of the conditions in this calculation set, radiation is either dominant or comparable to conduction, as illustrated in Figure 8. However, when the actual surface area of the particles compared to the flame front is considered, the value of F decreases from unity to approximately 0.35 and 0.038 when the flame is 1 and 10 mm thick, respectively. This factor will drive the ratio from (4) towards conduction. Therefore, if the flame thickness is in fact on the order of several millimeters or larger, it is unlikely that observed decrease in calculated flame speed is *dominated* by radiative losses unless the emissivity, temperature, and flame diameter (i.e., close to the wall) are large. Although further information is needed to determine the flame thickness accurately, this finding is still significant. Heat losses from sulfur dust flames may not be dominated by radiation which is contrary to what has been concluded about other dust flames (e.g., Al) where the product is also solid [17].

3.2.2. Discussion. The measured flame speeds from all of the test for both measurement techniques are shown in Figure 9. A large amount of data scatter is seen for both concentrations. It is believed that the range of flame speeds observed is at least in part due to the turbulence that remained in the system after the injection process. The flame speeds measured in each direction for a single experiment were observed to vary more than 50% in some cases. Moreover, there were instances where the signals from two probes in a single pair would indicate the flame had arrived at the same time. This observation is likely due to the flame approaching the ionization probe pair from a side-on approach rather than head-on as would be expected for a spherical flame. This point is further supported by the asymmetry observed by the highly irregular front seen by shadowgraph measurements [9].

The calculated laminar flame speeds from the pressure data and the ionization probes are plotted in Figure 9. Reasonable agreement is seen between the two measurement techniques. The flame speeds reported by Proust [8] were approximately 20% lower than the stoichiometric flame speed measured in the current work. This result suggests that it is *plausible* to use pressure-time data to estimate laminar flame speed. The higher flame speeds measured here are likely in part due to increased turbulence here, although it is difficult to prove without any doubt, because the level of turbulence was not measured in either study. Natural convection potentially also played a role. The burning sulfur particles produce hot gases, which of course will rise. The upward draft will then distort the flame front potentially increasing the surface area. Evidence of the effect of natural convection can be observed in Figure 2 where the flame has clearly propagated upwards more than downwards.

Therefore, it is somewhat inappropriate to use this technique to determine the *laminar* flame speed because of how both turbulence and natural convection effect the flame shape. It better represents the flame speed of an equivalent spherical flame with the same mass consumption rate. With that being said, the pressure-time data does provide a measure of a flame speed based upon the degree

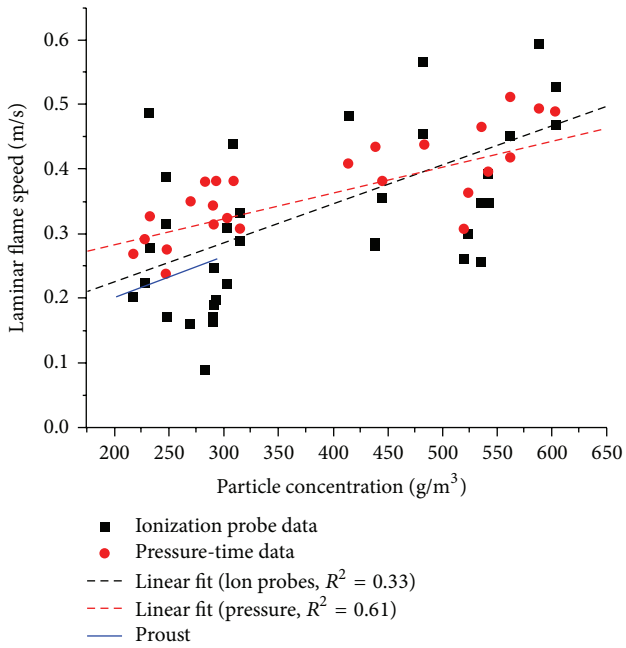

FIGURE 9: Comparison of the flame speed determined by the ionization probes, pressure-time data, and work from Proust [8].

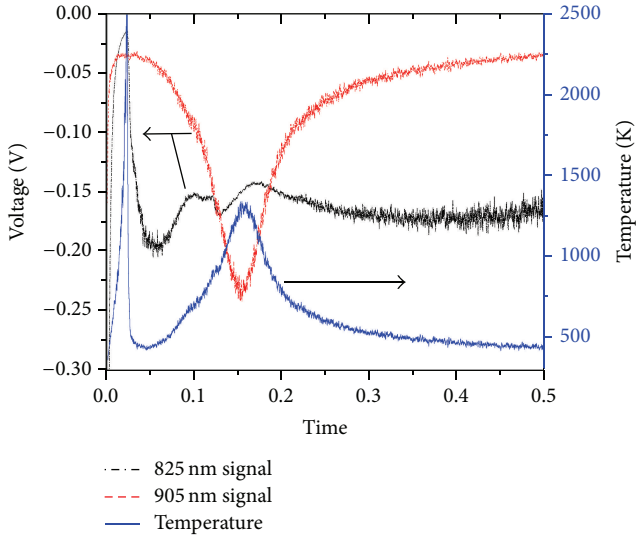

FIGURE 10: Representative filtered signals and calculated temperature for the PMT pyrometer.

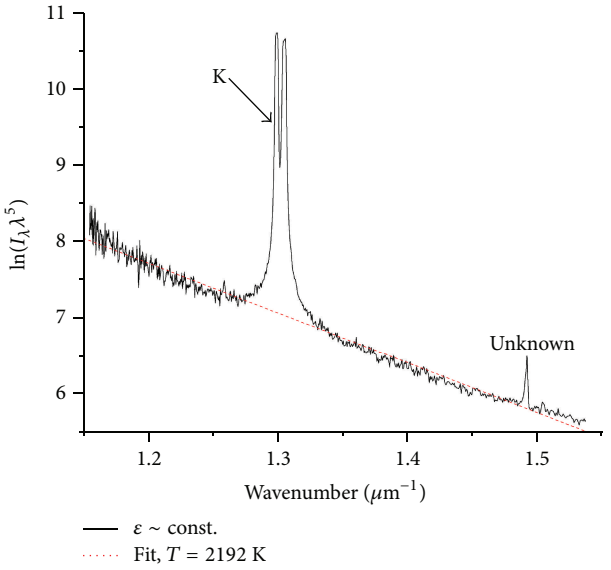

FIGURE 11: Fit of the thermal background from the Jaz spectrometer to determine temperature.

of turbulence. This result should still allow comparisons of flames in different conditions to be compared as long as the degree of turbulence is kept constant (i.e., injection parameters, ignition delay, and energy).

3.3. Flame Temperature. The temperature of the sulfur flames were measured by thermocouple and pyrometry. Both measurements were used to determine the peak temperature. The thermocouple provided the peak temperature locally, while pyrometry measurements indicated the peak temperature within the field of view of the pyrometer. The spatially integrated pyrometry signal is always biased towards the hottest regions due to the strong temperature dependence on the intensity of thermal radiation. Pyrometry data was collected with the 3-color PMT pyrometer and the Jaz Ocean Optics spectrometer. It should be noted that only the 825 nm and 905 nm signals were used because the 700 nm channel did not provide a sufficient signal level. The integration time for all data collected by the spectrometer was 10 ms.

Representative traces of the time-resolved data provided by the PMT pyrometer are displayed in Figure 10 with the calculated temperature using the gray body approximation. The early peak seen in Figure 10 was due to the emission from the pyrotechnic igniter. It was observed that the maximum temperature from the sulfur explosion occurred near the time that the rate of pressure rise was maximum. The peak temperature was recorded for each experiment.

Figure 11 shows a spectrum taken from the Jaz spectrometer. A gray body was believed to be the most appropriate assumption for the spectral emissivity because the λ^{-1} or λ^{-2} may not be appropriate for all materials [18] and the large optical depths produced by the dust cloud [19]. The measured peak temperatures from pyrometry and the thermocouples are shown in Figure 12. Only thermocouple data was obtained from the 10% oxygen tests, because the pyrometry signals were very weak and much lower than the noise level. The PMT pyrometer was used only for the 21% because of a spectral interference near 900 nm when the oxygen level was increased to 42% by volume. The thermal background from the Jaz spectrometer was fit for each of the tests for the oxygen-enriched conditions. As such, no time-resolved data were obtained for these conditions.

The dashed lines represent the maximum flame temperatures calculated under equilibrium conditions. The temperature was adjusted by considering the heat absorbed

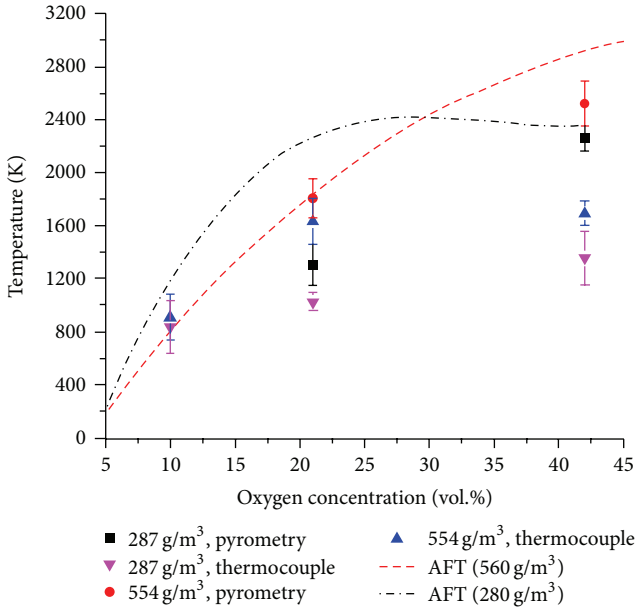

FIGURE 12: Temperature measurements of sulfur dust explosions.

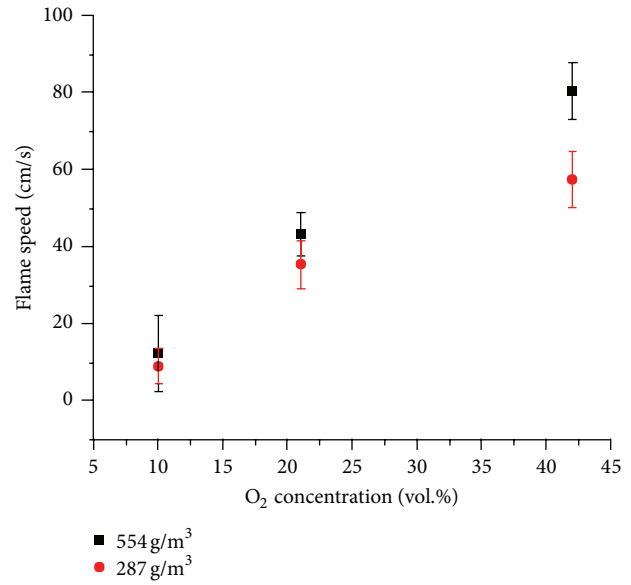

FIGURE 13: Flame speed measurements by analysis of pressure-time data for sulfur dust explosions.

by the anticaking agent. This change in temperature was minimal (typically less than 10 K). It should be noted that this adjustment is a first-order approximation since it did not include the equilibrium composition to be recalculated at the final temperature.

It was observed that the peak temperature steadily increased for the lower particle concentration from approximately 800 K to about 1300 K for the thermocouple measurements (corrected for radiative losses) as the oxygen content was increased from 10% to 42%. The increase in temperature from 21% to 42% oxygen from the pyrometry measurements was much greater as the maximum temperature exceeded 2000 K. This large difference is likely due to the fact that pyrometry measurements are biased towards the highest temperatures within the field-of-view while the thermocouples measured the local temperature.

A large temperature difference between the pyrometry and thermocouple measurements was also seen for the 21% and 42% oxygen tests at the higher particle loading. The temperature was observed to increase with particle loading for all oxygen concentrations. The average peak temperature for the 10% oxygen case was the lowest of the conditions for the 560 g/m^3 tests at 909 K.

The increase in temperature as oxygen concentration increased was likely due to the amount of energy liberated in each condition. The pressure data indicated that the maximum pressure rise (i.e., heat release), Figure 5, increased with oxygen concentation.

3.4. Flame Speed. Since the pressure-time data was determined to be an accurate way of measuring flame speed within the constant volume explosion chamber, it was decided to use that diagnostic to determine how particle and oxygen concentrations affected the flame speed. The same approach that was used to determine flame speed, as discussed above, was applied to the other conditions. The data for all of the particle and oxygen concentrations are summarized in Figure 13.

The individual data points for the 21% oxygen case were displayed in the previous section (see Figure 9). The averages at that oxygen concentration also includes additional data points taken after the completion of that portion of the work. A monotonic increase in flame speed was observed with an increase in oxygen concentration. A similar trend is shown in Figure 6 for the $(dP/dt)_{\max}$ data. Since the flame speed was calculated from the pressure data (and S_L scales with dP/dt), it is expected to see a similar dependence. For a given oxygen concentration, the higher particle loading condition (i.e., higher equivalence ratio) has a greater flame speed.

4. Combustion Mechanism Discussion

Gas-phase emission from sulfur oxides and S_2, as reported in [9], suggests that sulfur has a gas-phase component, but the extent of the gas-phase chemistry is unknown. However, the data do not explicitly suggest anything about the limiting process(es) during combustion, namely, if sulfur burns in a kinetically or diffusion limited manner.

4.1. Damköhler Number Analysis. Calculation of the key Damköhler number will aid in this discussion. This Damköhler number is the ratio of the chemical and diffusion time scales. A chemical time scale was determined by simulating an adiabatic, constant volume, perfectly-stirred reactor (PSR) with the SO_x mechanism from University of Leeds [12]. The ratios of sulfur, oxygen, and nitrogen that were present in the chamber after injection under atmospheric pressure were used as the initial conditions.

Table 1: Summary of the normalized Damköhler numbers.

	10% O_2	21% O_2	42% O_2
280 g/m^3	0.12	1.00	0.48
560 g/m^3	0.80	1.00	7.00

An initial temperature of 1300 K was needed to start the reaction. The time step was set to 1 microsecond. The chemical time scales were taken as the time it takes for the temperature to go from 10% to 90% of the total temperature change. The temperature change was the difference from 1300 K to the adiabatic flame temperature.

The diffusion time scale is inversely proportional to the diffusion coefficient, D, which was calculated from kinetic theory [20]. The binary diffusion coefficient of oxygen through nitrogen was calculated using the measured peak temperatures. The diffusion coefficient scales as $T^{1.65}$ and $MW^{-0.5}$. Because of this scaling, even if the temperature were to increase by 1700 K (bringing the temperature up to about 3100 K, the adiabatic flame temperature, for the hottest measured condition), the diffusion time scale would only decrease by about a factor of about 2.8. Similarly, if the diffusion of two other species besides O_2 and N_2 were considered (i.e., SO, SO_2, and S_2), the diffusion time scale would change by less than a factor of 2 (increase or decrease). Therefore, the diffusion coefficient will not change significantly (i.e., an order of magnitude) for mixtures of sulfur compounds, oxygen, and nitrogen. The pressure was taken as 1 atm for this calculation. The reasoning for this assumption was that at the time when the flame front passed the thermocouples and ionization probes, the pressure within the chamber had not significantly risen.

The Damköhler numbers calculated are relative to one another (i.e., not absolute) to eliminate concerns on the appropriate area to use to nondimensionalize the value and since the maximum pressure does not change substantially (i.e., less than an order of magnitude). The Da numbers shown in Table 1 are normalized to the value at 21% O_2 at each respective particle concentration so that individual values have no meaning, but the relative change is important.

A significant increase (i.e., by an order of magnitude) in Da is seen as the oxygen concentration increased from 10% to 21% for the lower particle concentration. A similar increase is observed for the 560 g/m^3 concentration as the oxygen content rises from 21% to 42%. This increase suggests that as the oxygen concentration increases, diffusion becomes more important which at first glance seems counterintuitive. Considering that the oxygen was not the only quantity that changed, this result is justified. The temperature also increased and that affects the chemistry more significantly than diffusion (i.e., exponentially versus $T^{1.65}$). The exponent on temperature (1.65) includes the temperature dependence from the collision integral [21]. The more intriguing aspect of this observation is that for both of the particle loadings, diffusion becomes more important as the flame transitions from fuel-rich conditions to stoichiometric. Stoichiometry for the 280 g/m^3 and 560 g/m^3 concentrations is when there is 21% and 42% oxygen by volume, respectively.

Table 2: Flame speed scaling in the diffusion limit.

	$V_{10\%}/V_{21\%}$	$V_{21\%}/V_{21\%}$	$V_{42\%}/V_{21\%}$
280 g/m^3	0.64	1.00	1.73
560 g/m^3	0.52	1.00	1.43

Table 3: Flame speed scaling in the kinetic limit.

	$V_{10\%}/V_{21\%}$	$V_{21\%}/V_{21\%}$	$V_{42\%}/V_{21\%}$
280 g/m^3	0.89	1.00	1.15
560 g/m^3	0.85	1.00	1.09

Table 4: Measured flame speed ratios.

	$V_{10\%}/V_{21\%}$	$V_{21\%}/V_{21\%}$	$V_{42\%}/V_{21\%}$
280 g/m^3	0.25	1.00	1.62
560 g/m^3	0.29	1.00	1.86

4.2. Flame Speed Scaling Analysis. The above discussion only provided insight into how the flames in each condition burned relative to one another. Analysis of the flame speed and temperature can be used to further specify the combustion mechanism and any limiting phenomena.

The scaling of the flame speed should be dependent on the burning mechanism. Landau and Lifshitz [22] state that the flame speed for a thermally driven combustion wave scales as $(\alpha/\tau_{\text{comb}})^{0.5}$, where τ_{comb} is a combustion time scale. Goroshin et al. [23] argued that for a diffusion limited flame, τ_{comb} scales inversely proportional to the diffusion coefficient of the gas. If the flame is diffusion limited, the flame speed should scale as $(\alpha D)^{0.5}$. Goroshin et al. [23] contended that if this thermally driven flame is kinetically limited, the difference in mass diffusivity of the gas mixtures (i.e., in each condition) should not play a role, thus the flame speed should scale with $(\alpha)^{0.5}$. This logic was used for the current work. The theoretical scaling for the diffusion and kinetically limited flames are shown in Tables 2 and 3, respectively. The velocity ratios from the data of the current work is displayed in Table 4.

It is observed that the ratio of experimentally measured velocities from the 21% and 42% oxygen cases (for both particle concentrations) are much closer to the ratio predicted by the diffusion limited theory. This result, in conjuction with the previous discussion, suggests that oxygen enriched sulfur dust flames burn in the diffusion limit.

Intuitively, it would be expected that an oxygen enriched flame would burn in the kinetic limit since a higher concentration of oxygen is closer to the particle surface and potentially significantly reducing the diffusion time scale. However, the oxygen concentration is only one aspect of these flames. The temperature measurements show that the flame burns hotter as more oxygen was added to the system. The diffusion time scale does decrease with temperature ($T^{1.65}$), but it is not affected as much as the kinetics, which scale exponentially with temperature. The increase in temperature

causes the chemistry to occur much faster, resulting in the diffusion process to be the limiting step.

Decreasing the oxygen concentration to 10% does not fit the scaling ratios predicted by kinetically or diffusion limited flame. The experiments with higher oxygen concentrations produced very consistent data whereas the 10% oxygen concentrations had a larger spread. The larger spread is not well represented by the data shown here. On multiple occasions, the 10% oxygen tests did not ignite (for both powder concentrations). It is possible that perhaps a flammability unit was approached by these oxygen depleted conditons.

4.3. Group Combustion Regime. Finally one must determine if the dust particles burn independently of each other. So a second condition that must be determined is the droplet spacing. The droplet combustion analysis assumes that there are no interactions with other particles [24]. The spray combustion community uses a group combustion number to estimate if the particles burn individually or together within a larger group flame. A group combustion number is defined by Glassman and Yetter [25] as follows:

$$G = 3\left(1 + 0.276\mathrm{Re}^{0.5}\mathrm{Sc}^{0.5}\mathrm{Le}N^{2/3}\right)\frac{R}{S}, \quad (5)$$

where Sc is the Schmidt number (ratio of momentum and mass diffusivities), Le is the Lewis number (ratio of thermal and mass diffusivities), N is the number of particles, R is the particle radius, and S is the average particle spacing [25]. The ratio of R and S is equal to the cube root of the quotient of the particle mass loading density (i.e., g/m^3) and the particle density [26] and is on the order of 0.1 for the conditions tested in this work. The number of particles within the chamber for a given test is off the order of 10^8-10^9. Both Sc and Le will be on the order of 0.1 to 1. The Reynolds number is unknown because the velocity was not measured but it is likely orders of magnitude larger than 10^{-8}-10^{-9}. Therefore, using (5), G will be much greater than 10^{-2}. A group number of less than 10^{-2} is specified for individually burning particles to occur [25].

5. Conclusions

Constant volume sulfur dust explosions were investigated. Measurements of flame speed using ionization probes showed reasonable agreement to the calculated speed from the pressure time data. Although there was agreement, it is inappropriate to call the quantity laminar flame speed because of the turbulence in the system. Flame speed was observed to range from 9 cm/s with 10% oxygen for both particle concetrations studied to as high as 80 cm/s in 42% oxygen for 554 g/m^3 of sulfur. The flame speed also increased with particle concentration which may be attributed to a shorter interparticle distance at higher concentrations. The temperature was measured to vary from approximately 800 K for both particle concentrations to approximately 2200 and 2600 for 287 g/m^3 and 554 g/m^3, respectively. Flame speed and temperature were not observed to be a function solely on equivalence ratio but rather dependent on the concentrations of sulfur and oxygen. Further analysis concluded that diffusion became the limiting process as the stoichiometry transitioned from fuel-rich to stoichiometric.

Conflict of Interests

The authors declare that there is no conflict of interests regarding the publication of this paper.

Acknowledgments

This work was funded by DTRA Grant HDTRA1-11-1-0014 under project manager Dr. Suhithi Peiris. The authors would like to thank undergraduate students Sasank Vemulapati and Chris Murzyn for their assistance. This work was carried out in part in the Frederick Seitz Materials Research Laboratory Central Facilities at the University of Illinois at Urbana, Champaign.

References

[1] J. O. Nriagu, Ed., *Sulfur in the Environment, Part I: The Atmospheric Cycle*, John Wiley and Sons, 1978.

[2] B. Setlow, C. A. Loshon, P. C. Genest, A. E. Cowan, C. Setlow, and P. Setlow, "Mechanisms of killing spores of *Bacillus subtilis* by acid, alkali and ethanol," *Journal of Applied Microbiology*, vol. 92, no. 2, pp. 362–375, 2002.

[3] D. Allen, *Optical combustion measurements of novel energetic material in a heterogeneous shock tube [M.S. thesis]*, University of Illinois, Mechanical Science and Engineering, Champaign, Ill, USA, 2012.

[4] S. Zhang, M. Schoenitz, and E. L. Dreizin, "Iodine release, oxidation, and ignition of mechanically alloyed Al-I composites," *The Journal of Physical Chemistry C*, vol. 114, no. 46, pp. 19653–19659, 2010.

[5] B. R. Clark and M. L. Pantoya, "The aluminium and iodine pentoxide reaction for the destruction of spore forming bacteria," *Physical Chemistry Chemical Physics*, vol. 12, no. 39, pp. 12653–12657, 2010.

[6] S. A. Grinshpun, A. Adhikari, M. Yermakov et al., "Inactivation of aerosolized *Bacillus atrophaeus* (BG) endospores and MS2 viruses by combustion of reactive materials," *Environmental Science & Technology*, vol. 46, no. 13, pp. 7334–7341, 2012.

[7] M. Clemenson, *Explosive initiation of various forms of the ti/2b energetic system [M.S. thesis]*, University of Illinois at Urbana-Champaign, Mechanical Science and Engineering, 2012.

[8] C. Proust, "Flame propagation and combustion in some dust-air mixtures," *Journal of Loss Prevention in the Process Industries*, vol. 19, no. 1, pp. 89–100, 2006.

[9] J. Kalman, *Experimental investigation of constant volume sulfur dust explosions [Ph.D. thesis]*, University of Illinois at Urbana-Champaign, 2014.

[10] M. R. S. Nair and M. C. Gupta, "Burning velocity measurement by bomb method," *Combustion and Flame*, vol. 22, no. 2, pp. 219–221, 1974.

[11] D. Goodwin, *Cantera: An Object-Oriented Software Toolkit for Chemical Kinetics, Thermodynamics, and Transport Processes*, Caltech, Pasadena, Calif, USA, 2009.

[12] T. Ziehn and A. S. Tomlin, "A global sensitivity study of sulfur chemistry in a premixed methane flame model using HDMR,"

International Journal of Chemical Kinetics, vol. 40, no. 11, pp. 742–753, 2008.

[13] S. Gordon and B. J. McBride, "Computer program for calculation of complex chemical equilibrium compositions and applications," NASA Reference Publication 1311, NASA, Washington, DC, USA, 1996.

[14] K. L. Cashdollar, "Flammability of metals and other elemental dust clouds," *Process Safety Progress*, vol. 13, no. 3, pp. 139–145, 1994.

[15] A. E. Dahoe and L. P. H. de Goey, "On the determination of the laminar burning velocity from closed vessel gas explosions," *Journal of Loss Prevention in the Process Industries*, vol. 16, no. 6, pp. 457–478, 2003.

[16] C. C. M. Luijten, E. Doosje, and L. P. H. de Goey, "Accurate analytical models for fractional pressure rise in constant volume combustion," *International Journal of Thermal Sciences*, vol. 48, no. 6, pp. 1213–1222, 2009.

[17] P. R. Santhanam, V. K. Hoffmann, M. A. Trunov, and E. L. Dreizin, "Characteristics of aluminum combustion obtained from constant-volume explosion experiments," *Combustion Science and Technology*, vol. 182, no. 7, pp. 904–921, 2010.

[18] J. Kalman, N. Glumac, and H. Krier, "High temperature metal oxide spectral emissivities for pyrometry applications," *AIAA Journal of Thermophysics and Heat Transfer*. Submitted.

[19] J. Kalman, D. Allen, N. Glumac, and H. Krier, "Optical depth effects on aluminum oxide spectral emissivity," *Journal of Thermophysics and Heat Transfer*, vol. 29, no. 1, pp. 74–82, 2015.

[20] N. M. Laurendeau, *Statistical Thermodynamics: Fundamentals and Applications*, Cambridge University Press, New York, NY, USA, 2010.

[21] L. Monchick and E. A. Mason, "Transport properties of polar gases," *The Journal of Chemical Physics*, vol. 35, no. 5, pp. 1676–1697, 1961.

[22] L. Landau and E. Lifshitz, *Fluid Mechanics*, Pergamon Press, 1959.

[23] S. Goroshin, F.-D. Tang, A. J. Higgins, and J. H. Lee, "Laminar dust flames in a reduced-gravity environment," *Acta Astronautica*, vol. 68, no. 7, pp. 656–666, 2011.

[24] S. R. Turns, *An Introduction to Combustion: Concepts and Applications*, McGraw-Hill Series in Mechanical Engineering, McGraw-Hill Education, 2000, http://books.google.com.eg/books?id=sqVIPgAACAAJ&redir_esc=y.

[25] I. Glassman and R. Yetter, *Combustion*, Academic Press, 2008.

[26] R. K. Eckhoff, "Chapter 4—propagation of flames in dust clouds," in *Dust Explosions in the Process Industries*, pp. 251–384, Gulf Professional Publishing, Burlington, Vt, USA, 3rd edition, 2003.